science, engineering and health studies

Research Article

Science, Engineering and Health Studies
https://lio1.tci-thaijo.org/index.php/sehs
ISSN (Online): 2630-0087

Biomechanical evaluation of conventional locking compression plate and double locking compression plate combined with locking screw use to stabilize midshaft ulna fracture: A finite element study

Potsadom Moraksa[1], Sujin Wanchat[1,2], and Nattapon Chantarapanich[1,2]*

[1] Department of Mechanical Engineering, Faculty of Engineering at Sriracha, Kasetsart University, Chonburi 20230, Thailand
[2] Digital Industrial Design and Manufacturing Research Unit, Faculty of Engineering at Sriracha, Kasetsart University, Chonburi 20230, Thailand

ABSTRACT

This study explored the impact of midshaft ulna fractures on biomechanical performance of double locking compression (D-LCP) in comparison to conventional locking compression plates, utilizing finite element method. The study included transverse middle fractures stabilized with titanium implants, involving models of midshaft ulna and two fixation plates (D-LCP implant and C-LCP implant) created and aligned virtually using CAD. Four-node tetrahedral elements were employed in the finite element model, and regular daily activity loading conditions were applied to each model at axial compression, axial torsion, and lateral bending. EQV stress was observed around the distal screw contact in both C-LCP and D-LCP models, with D-LCP exhibiting lower EQV stress than C-LCP, particularly under axial compression. The D-LCP cases demonstrated less bone fracture displacement compared to C-LCP cases, providing valuable insights. Additionally, the bone stress in D-LCP revealed significantly lower levels compared to C-LCP.

Keywords: double locking compression; ulna fracture; biomechanics

***Corresponding author**:
Nattapon Chantarapanich
nattapon@eng.src.ku.ac.th

***Received**: 1 April 2024*
***Revised**: 10 June 2024*
***Accepted**: 18 June 2024*
***Published**: 29 December 2024*

***Citation**:
Moraksa, P., Wanchat, S., and Chantarapanich, N. (2024). Biomechanical evaluation of conventional locking compression plate and double locking compression plate combined with locking screw use to stabilize midshaft ulna fracture: A finite element study. Science, Engineering and Health Studies, 18, 24040007.

1. INTRODUCTION

The body's response to protect against blunt force injuries typically involves raising the forearm to guard the head or face. High energy produced from the object striking the forearm may result in severe trauma (Atkin et al., 1995; De Buren, 1962). One common incident is an ulna shaft fracture (nightstick fracture) (Goel et al., 1991), which

accounts for around 22% of upper extremity trauma (Altner and Hartmann, 1972).

Treatment for ulna shaft fracture can utilize either non-operative or operative techniques (Baratz, 2021). The non-operative technique is limited to minimal displacement and angulation (Altner and Hartmann, 1972; Atkin et al., 1995; Corea et al., 1981; Gebuhr et al., 1992), whereas the operative technique is normally suited to managing large displaced fractures (Brakenbury et al., 1981). The non-operative technique typically requires internal fixation to stabilize the fracture and align the fragment. These fixations use plate-screw fixation and intramedullary rods (Brakenbury et al., 1981; Dymond, 1984; Ostermann et al., 1994).

Among of these fixations, a plate-screw is commonly used to manage fractures due to its ease of operation, and it achieves more desired long-term clinical outcomes compared to using an intramedullary rod (Hooper, 1974; Hussain et al., 2018). Some studies have suggested the approach of a small dynamic compression plate (DCP) with six screw holes combined with a compression screw to treat simple ulna shaft fractures (Hadden et al., 1983), which resulted in a 97% union rate. However, besides its desirable success rate, some clinical cases using DCP have had complications with screw withdrawal. A locking compression plate (LCP) is therefore more commonly used. In addition, LCP demonstrates superior biomechanical results in axial compression compared to DCP (Cronier et al., 2010; Larson and Rizzo, 2007; Snow et al., 2008; Xiong et al., 2009).

Despite its performance advantage, LCP still has limitations such as a limited number of screws, particularly in short ulnas or fractures close to the epiphyseal. This could reduce bone-implant construct stiffness and strength. To enhance LCP performance, a double-locking combination hole has been introduced, but its biomechanical performance has yet to be properly evaluated. This is an aim of this study which seeks to address this issue by comparing biomechanical performance under different loading conditions of the conventional locking technique and the novel locking technique of LCP by means of a finite element (FE) method.

2. MATERIALS AND METHODS

This study was approved by the institutional ethics committee of the authors' institution (study code KUREC-SRC 66/010). The study involved the construction of three-dimensional (3D) models of the ulna and implants. All FE model preparation and analyses were performed in FE pre-processing (Patran, MSC Software Inc., USA) and FE commercial software packages (Marc Mentat, MSC Software Inc., USA).

2.1 CAD model of ulna and implant

A meticulously prepared ulna bone was acquired by collecting its precise coordinates using a spiral computed tomography (CT) scanner. The slice data images obtained by the process were stored in the digital imaging and communications in medicine (DICOM) file format. These images were imported into 3D Slicer (slicer.org) (Fedorov et al., 2012), an image-processing software tool in order to create a 3D model of an ulna. This imaging process entailed the careful selection of the ulna bone through thresholding proper Hounsfield unit (HU) range in the set of visualization image data. This subsequently resulted in a 3D ulna model with an intramedullary canal, with a length of 305.8 mm. The average cortical thickness at epiphysis was 2 mm, while the cortex at diaphysis was 4 mm. The cancellous layer of each epiphysis was within the intramedullary canal of the ulna. The length of the cancellous layer was 45 mm measured from the joint surface. Since the analysis focused on transverse fracture with a fracture gap of 10 mm (Santos et al., 2016; Xiong et al., 2009), the ulna was divided in the middle, resulting in proximal and distal fragments.

Two fixation plates were used in this study, a conventional locking compression plate (C-LCP) and a double locking compression plate (D-LCP). The C-LCP was 111 mm long, 3.4 mm thick, and featured eight combination holes. The D-LCP was identical in length, thickness, and combination hole diameters to the C-LCP. There were six double locking slots with 12 screws holes in total. For both plates, 5 mm diameter locking screws were employed. Screw and hole thread were omitted to simplify the calculation (Gee et al., 2021).

The symmetrical fixation of the C-LCP plate to both upper and lower bones was established on the ulna (Sarwar et al., 2021; Wagner, 2003). The plate was virtually placed on the ulna bone using CAD software. The designation of the screw is presented in Figure 1. A minimum of three screws were located on each fragment. Hence, there were eleven configurations for D-LCP and a single case for C-LCP.

2.2 FE model generations

An FE model of the ulna and the implant was created using a four-node tetrahedral element. This was accomplished through the application of an automatic mesh generation technique (Jitprapaikulsarn et al., 2021) (Patran, MSC Software Inc., USA). The element size within the holes of the LCP plate and the cortical bone was finer than in other areas. Different numbers of elements of the C-LCP case and D-LCP case No. 6 were tested under convergence study under 20N axial compression. Equivalent von Mises (EQV) stress was used to monitor the convergence. FE model generations are shown in Figure 2.

2.3 Material properties

All material properties assigned to the FE models were assumed to be homogeneous and linearly elastic. The cortical and cancellous bone models were anisotropic, whereas implants were assumed to be medical-grade titanium alloys. All material properties are shown in Table 1.

2.4 Boundary and contact conditions

The regular daily activity loading conditions of the ulna were assigned to each FE model, i.e., 20 N and 50 N axial compression, 1 N.m axial torsion, and 1 N.m lateral bending (Zhang et al., 2021). All degrees of freedom were constrained at the ulna proximal end, as shown in Figure 3.

2.5 Contact conditions

Contact conditions were established between each part of the model, specifying that the contact between the LCP plate and the ulna bone was defined with touch contact, with a coefficient of friction of 0.3, and screws were fixed to the ulna bone and LCP, defined as glue contact. The contact condition is shown in Table 2 (Jitprapaikulsarn et al., 2021).

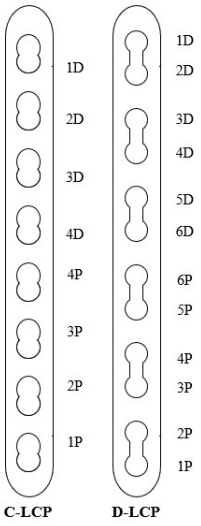

C-LCP	D-LCP no.01	D-LCP no.02	D-LCP no.03	D-LCP no.04	D-LCP no.05	D-LCP no.06	D-LCP no.07	D-LCP no.08	D-LCP no.09	D-LCP no.10	D-LCP no.11
1D	1D	1D	1D	1D	1D	1D	1D	1D	1D	1D	1D
X	2D	2D	2D	2D	2D	2D	2D	2D	2D	2D	2D
2D	3D	3D	3D	3D	3D	3D	3D	3D	3D	3D	3D
X	4D	4D	4D	4D	4D	4D	4D	4D	4D	4D	4D
3D	5D	5D	5D	5D	5D	5D	5D	5D	5D	5D	5D
3P	5P	5P	5P	5P	5P	5P	5P	5P	5P	5P	5P
X	4P	4P	4P	4P	4P	4P	4P	4P	4P	4P	4P
2P	3P	3P	3P	3P	3P	3P	3P	3P	3P	3P	3P
X	2P	2P	2P	2P	2P	2P	2P	2P	2P	2P	2P
1P	1P	1P	1P	1P	1P	1P	1P	1P	1P	1P	1P

Screw Configurations patterns

Figure 1. Screw configuration patterns

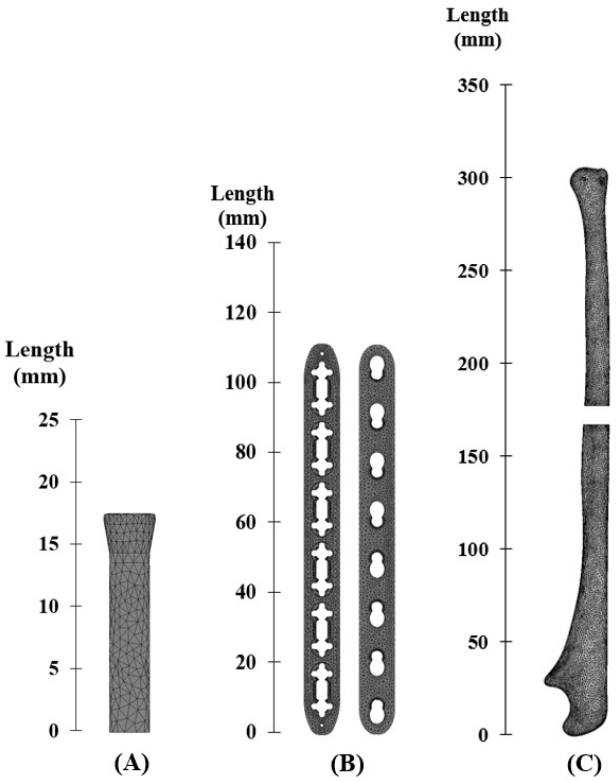

Figure 2. FE models of a (A) locking screw, (B) D-LCP/ C-LCP, and (C) ulna bone using MSC Patran software

Table 1. Material properties (Coates et al., 2012; Kanjanamekanant, 2020)

Material	Elastic modulus (MPa)	Shear modulus (MPa)	Poisson's ratio
Cortical bone	E_1 = 16,000	G_{12} = 3,200	υ_{12} = 0.30
	E_2 = 6,900	G_{23} = 3,300	υ_{23} = 0.45
	E_3 = 6,300	G_{31} = 3,600	υ_{31} = 0.30
Cancellous bone	E_1 = 800	G_{12} = 260	υ_{12} = 0.30
	E_2 = 600	G_{23} = 520	υ_{23} = 0.30
	E_3 = 600	G_{31} = 370	υ_{31} = 0.30
Titanium	E = 110,000		υ = 0.33

Note: 1=axial direction, 2=radial direction, and 3=circumference direction

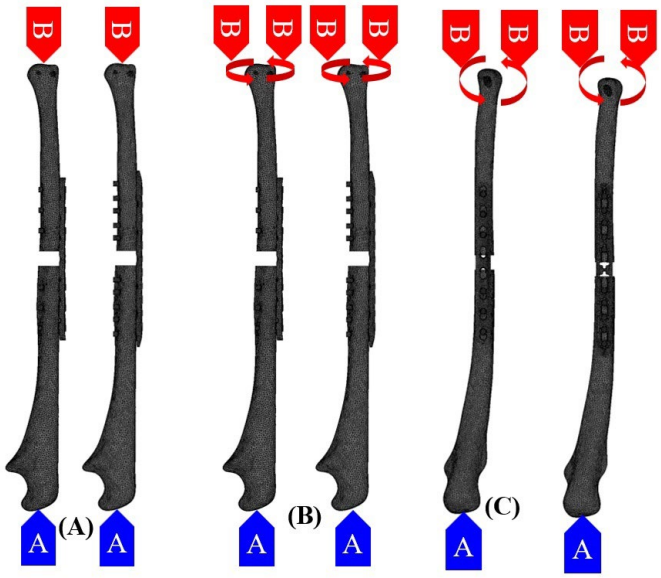

Figure 3. Boundary condition of FE analysis: (A) axial compression, (B) axial torsion, and (C) lateral bending

Table 2. Contact conditions

Contact condition	Distal cortical	Distal cancellous	Screw upper	Plate	Screw lower	Proximal cancellous	Proximal cortical
Distal cortical		*Glue*	*Glue*	*Touch*	-	-	-
Distal cancellous	*Glue*		-	-	-	-	-
Screw upper	*Glue*	-		*Glue*	-	-	-
Plate	*Touch*	-	*Glue*		*Glue*	-	*Touch*
Screw lower	-	-	-	*Glue*		-	*Glue*
Proximal cancellous	-	-	-	-	-		*Glue*
Proximal cortical	-	-	-	*Touch*	*Glue*	*Glue*	

3. RESULTS

3.1 Convergence test results

The number of elements greater than 195,062 (48,141 nodes) for the C-LCP and greater than 193,717 (48,593 nodes) for the D-LCP produced 6.6% and 7.7% difference in maximum EQV stress, respectively (Jitprapaikulsarn et al., 2021) Thus, these number of elements and corresponding number of nodes were employed for the FE study. The results are shown in Figure 4.

3.2 Stress distribution on implant

The maximum EQV stress occurred around the contact of the distal screw in both the C-LCP and D-LCP models. In axial compression, six or more screws (Case No. 1-11) reduced EQV stress for D-LCP compared to C-LCP by 10.30–55.80%. For axial torsion, although the 8-screw configuration without 2D/2P positioning reduced EQV stress compared to other D-LCP cases, it was still greater than C-LCP. The results are presented in Figure 5 and Table 3.

In lateral bending, 6 and 8-screw configurations without 2D/2P screws could lower EQV stress compared to other D-LCP cases with the same number of screws. Neither 6, 8, or 10 screws when positioned at 2D/2P notably raised stress levels.

3.3 Fracture displacement

The analysis of bone fracture displacement provided valuable insights into fracture stability. D-LCP cases provided less displacement than the C-LCP case. Under axial compression, a six-screw fixation without 5D/5P (Case No. 7, 8, and 10) reduced D-LCP displacement compared to other D-LCP cases. Eight screws with the inclusion of 3D/3P and 5D/5P positions could also lower displacement. The ten-screw D-LCP provided a displacement value comparable to other cases. The results are shown in Table 4.

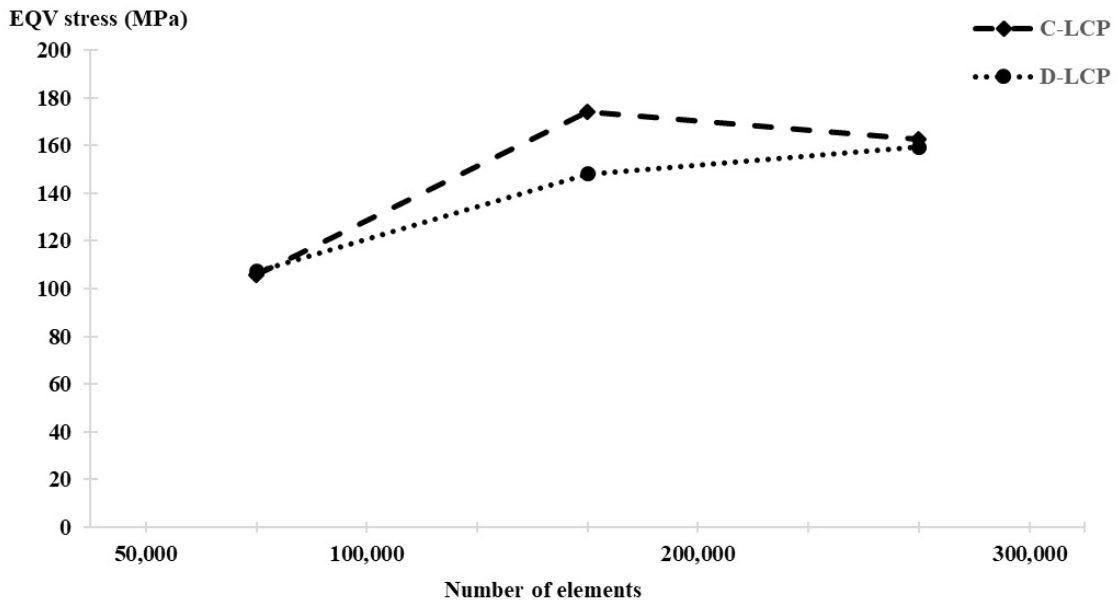

Figure 4. Convergence test results

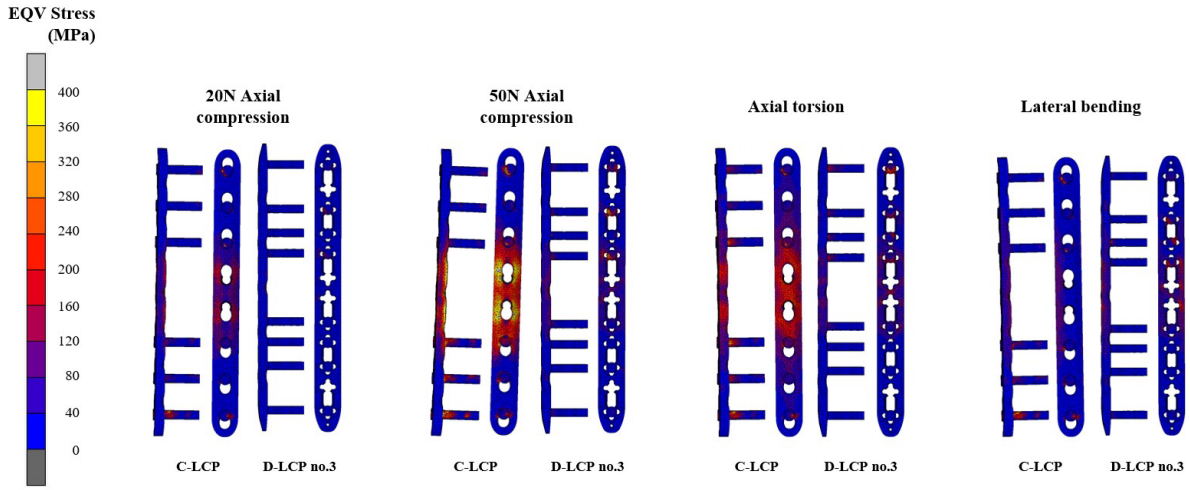

Figure 5. Implant stress (MPa)

Table 3. Stress on implant (MPa)

Loading condition	C-LCP	D-LCP										
		No.1	No.2	No.3	No.4	No.5	No.6	No.7	No.8	No.9	No.10	No.11
20N axial compression	174.90	101.90	157.20	97.95	94.15	129.40	148.00	96.32	102.50	145.70	79.56	97.35
50N axial compression	438.20	255.30	392.90	246.20	235.80	324.10	371.10	241.00	256.60	365.50	198.90	244.80
1N·m axial torsion	151.60	179.30	230.00	207.40	215.40	226.30	270.90	282.50	282.20	254.50	262.20	237.60
1N·m lateral bending	273.30	230.70	341.20	171.10	186.00	264.50	280.00	281.90	250.90	212.30	125.20	122.10

Table 4. Fracture displacement (mm)

Loading condition	C-LCP	D-LCP									
		No.1	No.2	No.3	No.4	No.5	No.6	No.7	No.8	No.9	No.10	No.11
20N axial compression	5.22	0.41	0.59	0.33	0.36	0.58	0.60	0.15	0.34	0.39	0.98	5.22
50N axial compression	12.99	1.04	1.48	0.82	0.90	1.45	1.50	0.37	0.84	0.99	2.49	12.99
1N·m axial torsion	4.61	0.24	0.39	0.18	0.21	0.37	0.36	0.44	0.28	0.27	0.25	4.61
1N·m lateral bending	7.81	1.44	1.81	1.14	1.43	1.98	1.89	1.94	1.82	1.15	3.01	7.81

In axial torsion, 6 and 8 screws without 2D/2P demonstrated less fracture displacement for both 6 and 8 screw configurations compared to other configurations with the same number of screws.

For lateral bending, 6 and 8 screws without a screw placed in 2D/2P could reduce fracture displacement. Ten screws resulted in comparable displacement to those of six and eight screw configurations.

3.4 Bone stress

D-LCP resulted in significantly lower bone stress than C-LCP. Under axial compression, the screws in D-LCP with 3D/3P (8 screws configuration) and 4D/4P positions (6 screws configuration) reduced the principal stress exhibited in bone compared to other D-LCP cases with the same screw length. In axial torsion, both six and eight screws yielded similar bone stress levels (6.24–10.03 MPa). Moreover, a comparable stress level was also observed in 6, 8, and 10 screws subjected to lateral bending. The results are presented in Figure 6 and Table 5.

4. DISCUSSION

Ulna fractures are typically treated with C-LPC plates, which has limitations in terms of screw placement and the number of screws that can be utilized. To address these constraints, a concept for a double locking combination hole was introduced in this study.

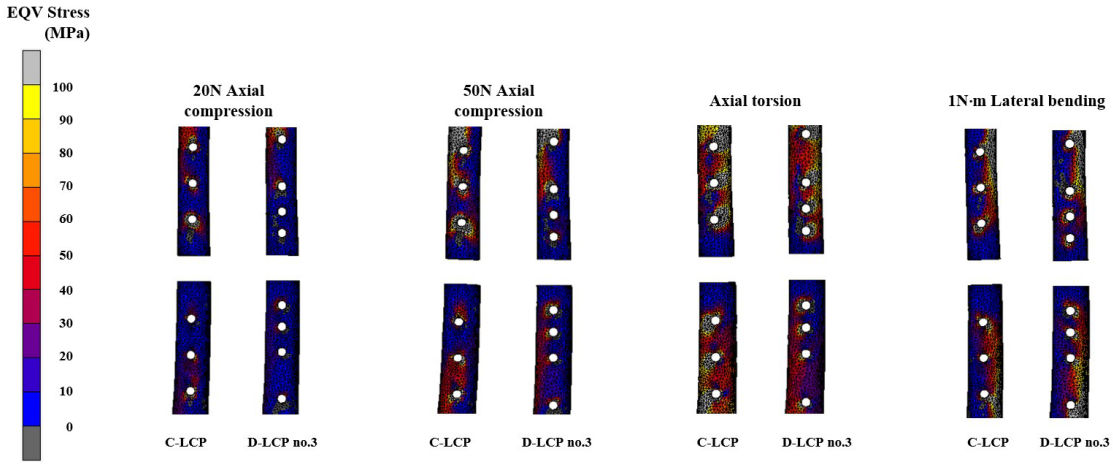

Figure 6. Bone stress (MPa)

Table 5. Bone stress (MPa)

Loading condition	C-LCP	D-LCP									
		No.1	No.2	No.3	No.4	No.5	No.6	No.7	No.8	No.9	No.10	No.11
20N axial compression	61.95	4.52	17.44	4.30	6.56	7.37	18.97	3.97	8.24	3.96	3.46	6.04
50N axial compression	114.90	11.32	43.60	10.77	16.42	18.45	47.49	9.94	20.64	9.92	8.68	15.17
1N·m axial torsion	62.74	11.70	9.78	6.24	6.62	8.04	10.03	9.75	7.57	7.61	8.31	7.84
1N·m lateral bending	62.76	11.02	9.90	17.95	11.47	9.14	12.45	12.39	11.04	12.21	11.58	9.45

EQV stress distribution on the implant was used to evaluate the risk of implant failure (Wang et al., 2020; Xue et al., 2024). From this study, it was found that D-LCP presented lower implant EQV stress than C-LCP. In axial compression, D-LCP reduced in EQV stress value by 10.30–55.80% and lateral bending by 8.20–55.30% compared to C-LCP, except for axial torsion testing. Yield stress of material refers to the minimum amount of stress a material must endure before it undergoes a significant, permanent deformation or a transition from elastic to plastic behavior (Egol et al., 2004). In this case, the yield stress of the implant material was 880 MPa (Bauccio, 1993; Ho et al., 1997). The findings from the D-LCP experiment held less significance. Axial compression occurs at a significantly lower level than the yield stress value by 55.35–90.96% and lateral bending by 61.23– 86.13%. Therefore, both implants are safe for axial loading.

For axial torsion, all D-LCP cases presented higher EQV stress than C-LCP. Due to D-LCP being designed with the concept of a double locking slot that increases screw positions and the number of screws, resulting in a stiffer locking system than C-LCP, the D-CLP experienced higher stress than the C-LCP implant. According to the findings of Collins et al. (2014) and Gardner et al. (2005), a fixation plate with a more rigid construction does not effectively withstand repetitive axial torsion and fails sooner than a less rigid construct. The axial torsion value is much lower than the yield stress (67.90–79.63%).

For lateral bending, a D-LCP configuration without 2D/2P screws could reduce EQV stress compared to other D-LCP or C-LCP configurations with an identical number of screws. Avoiding the 2D locking position can decrease implant stress due to its high stress indication. Stiffer constructions are indicated to be less effective in resisting lateral bending and axial torsion, potentially leading to earlier failure compared to constructs with less rigidity (Collins et al., 2014; Gardner et al., 2005). Activities involving axial torsion should be avoided, since it represents a critical loading condition for D-LCP.

Assessing fracture displacement was utilized in this study to evaluate the stability of the fracture. The plate fixation system exhibits a smaller maximum displacement, indicating not only improved construct stability but also reduced movement between the distal and proximal fragments (Zhang et al., 2021). Under all loading conditions, D-LCP presented lower displacement of the fracture between distal and proximal than C-LCP. Axial compression reduced in value by 88.40–97.10%, axial torsion by 90.40–97.30%, and lateral bending by 74.60–85.40%. In this case, the displacement of C-LCP in axial compression was 5.22–12.99 mm, axial torsion was 4.61 mm, and lateral bending was 7.81 mm.

The presence of bone stress indicates a high risk of secondary fractures, particularly within the cortical bone and screws. Under all loading conditions, the D-LCP consistently demonstrated significantly lower bone stress compared to the C-LCP. Despite being the same length as the C-LCP, the D-LCP utilizes a double locking slot design, allowing enhanced locking positions without requiring an increase in plate length. This enables an increase in the diversity of positions and the number of screw locks without the need to extend the length of the plate, thereby facilitating the convenience of developing shorter yet equally effective plate designs for future treatment. Moreover, reducing the length of the plate helps minimize the occurrence of unnecessarily large incisions during treatment. In this case, the yield stress of cortical bone is 114 MPa (Kutz, 2003; Murphy et al., 2016). For axial compression, D-LCP occurs at a level significantly lower than the cortical bone yield stress value by 58.34–96.96%, axial torsion by 89.74–94.53%, and lateral bending by 84.25–91.98% compared to C-LCP. Lower values for all loading conditions relative to cortical bone yield stress demonstrate a low risk of bone fracture.

This study utilized FE analysis to observe the biomechanics of bone-plate constructs. A linear element was employed in the FE simulation, since it produced results comparable to those with second order elements, while reducing computing time (Jiang et al., 2021). The study compared plate and screw positions. However, a limitation of this study is that no mechanical experiment was conducted. Another limitation is that the screws were positioned symmetrically, both above and below the fracture, with the fixation process commencing from the initial hole on either side of the plate's edge to ensure an evenly distributed pattern. Due to the extensive scope of case studies requiring analysis via the FE method, asymmetric considerations were omitted.

5. CONCLUSION

The focus of this study was on developing an innovative implant fixation plate D-LCP to treat ulna fractures. The study revealed that D-LCP exhibited significantly improved stability and fracture prevention capabilities compared to C-LCP. Additionally, this study recommends a fixation approach using six or eight screws, emphasizing specific screw placements while avoiding high stress fixation of 2D/2P positions (fixation pattern no. 3, 9, 10, and 11) to enhance the stability of fracture treatments. The results highlight the promising role of D-LCP in substantially enhancing the management of midshaft ulna fractures in clinical practice. These findings suggest the potential widespread adoption of the D-LCP concept into commercial applications.

ACKNOWLEDGMENT

This research is funded by Kasetsart University through the Graduate School Fellowship Program.

REFERENCES

Altner, P. C., and Hartmann, J. T. (1972). Isolated fractures of the ulnar shaft in the adult. *Surgical Clinics of North America*, 52(1), 155–170.

Atkin, D. M., Bohay, D. R., Slabaugh, P., and Smith, B. W. (1995). Treatment of ulnar shaft fractures: A prospective, randomized study. *Orthopedics*, 18(6), 543–547.

Baratz, M. E. (2021). Disorders of the forearm. In *Green's Operative Hand Surgery* (Wolfe, S. W., Pederson, W. C., Kozin, S. H., and Cohen, M S., Eds.), 8th, pp. 950–976. Philadelphia, PA: Elsevier.

Bauccio, M. (1993). *ASM Metals Reference Book*, 3rd, Ohio: ASM International. p. 614.

Brakenbury, P. H., Corea, J. R., and Blakemore, M. E. (1981). Non-union of the isolated fracture of the ulnar shaft in adults. *Injury*, 12(5), 371–375.

Coates, C., Goeser, P., Coates-Clark, C., and Jenkins, M. (2012). Impact response and simulation of damaged ulna with internal fixation. *Journal of Applied Biomechanics*, 28(3), 324–334.

Collins, M., Hart, A., Hines, J., Steffen, T., Harvey, E. J., and Martineau, P. A. (2014). Distal ulna fractures: A biomechanical comparison of locking versus nonlocking plating constructs. *Journal of Orthopaedic Trauma*, 28(8), 470–475.

Corea, J. R., Brakenbury, P. H., and Blakemore, M. E. (1981). The treatment of isolated fractures of the ulnar shaft in adults. *Injury*, 12(5), 365–370.

Cronier, P., Pietu, G., Dujardin, C., Bigorre, N., Ducellier, F., and Gérard, R. (2010). The concept of locking plates. *Orthopaedics & Traumatology: Surgery & Research*, 96(4), S17–S36.

De Buren, N. (1962). Causes and treatment of non-union in fractures of the radius and ulna. *The Journal of Bone and Joint Surgery British Volume*, 44–B(3), 614–625.

Dymond, I. W. (1984). The treatment of isolated fractures of the distal ulna. *The Journal of Bone and Joint Surgery British Volume*, 66–B(3), 408–410.

Egol, K. A., Kubiak, E. N., Fulkerson, E., Kummer, F. J., and Koval, K. J. (2004). Biomechanics of locked plates and screws. *Journal of Orthopaedic Trauma*, 18(8), 488–493.

Fedorov, A., Beichel, R., Kalpathy-Cramer, J., Finet, J., Fillion-Robin, J.-C., Pujol, S., Bauer, C., Jennings, D., Fennessy, F., Sonka, M., Buatti, J., Aylward, S., Miller, J. V., Pieper, S., and Kikinis, R. (2012). 3D slicer as an image computing platform for the quantitative imaging network. *Magnetic Resonance Imaging*, 30(9), 1323–1341.

Gardner, M. J., Brophy, R. H., Campbell, D., Mahajan, A., Wright, T. M., Helfet, D. L., and Lorich, D. G. (2005). The mechanical behavior of locking compression plates compared with dynamic compression plates in a cadaver radius model. *Journal of Orthopaedic Trauma*, 19(9), 597–603.

Gebuhr, P., Hölmich, P., Orsnes, T., Soelberg, M., Krasheninnikoff, M., and Kjersgaard, A. G. (1992). Isolated ulnar shaft fractures. Comparison of treatment by a functional brace and long-arm cast. *The Journal of Bone and Joint Surgery British Volume*, 74–B(5), 757–759.

Gee, A., Bougherara, H., Schemitsch, E. H., and Zdero, R. (2021). Biomechanical design using in-vitro finite element modeling of distal femur fracture plates made from semi-rigid materials versus traditional metals for post-operative toe-touch weight-bearing. *Medical Engineering & Physics*, 87, 95–103.

Goel, S. C., Raj, K. B., and Srivastava, T. P. (1991). Isolated fractures of the ulnar shaft. *Injury*, 22(3), 212–214.

Hadden, W. A., Reschauer, R., and Seggl, W. (1983). Results of AO plate fixation of forearm shaft fractures in adults. *Injury*, 15(1), 44–52.

Ho, C. Y., Holt, J. M., and Mindlin, H. (1997). *Structural Alloys Handbook*, West Lafayette, IN: Cindas/Purdue University.

Hooper, G. (1974). Isolated fractures of the shaft of the ulna. *Injury*, 6(2), 180–184.

Hussain, A., Nema, S. K., Sharma, D., Akkilagunta, S., and Balaji, G. (2018). Does operative fixation of isolated fractures of ulna shaft results in different outcomes than non-operative management by long arm cast? *Journal of Clinical Orthopaedics and Trauma*, 9(Suppl. 1), S86–S91.

Jiang, D., Zhan, S., Wang, L., Shi, L. L., Ling, M., Hu, H., and Jia, W. (2021). Biomechanical comparison of five cannulated screw fixation strategies for young vertical femoral neck fractures. *Journal of Orthopaedic Research*, 39(8), 1669–1680.

Jitprapaikulsarn, S., Chantarapanich, N., Gromprasit, A., Mahaisavariya, C., and Patamamongkonchai, C. (2021). Single lag screw and reverse distal femur locking compression plate for concurrent cervicotrochanteric and shaft fractures of the femur: Biomechanical study validated with a clinical series. *European Journal of Orthopaedic Surgery & Traumatology*, 31(6), 1179–1192.

Kanjanamekanant, K. (2020). Titanium and titanium alloys in implant dentistry. *Journal of the Dental Association of Thailand*, 70(2), 83–93. [in Thai]

Kutz, M. (2003). *Standard Handbook of Biomedical Engineering and Design*. New York: McGraw-Hill.

Larson, A. N., and Rizzo, M. (2007). Locking plate technology and its applications in upper extremity fracture care. *Hand Clinics*, 23(2), 269–278.

Murphy, W., Black, J., and Hastings, G. (2016). *Handbook of Biomaterial Properties*, 2nd, New York: Springer.

Ostermann, P. A., Ekkernkamp, A., Henry, S. L., and Muhr, G. (1994). Bracing of stable shaft fractures of the ulna. *Journal of Orthopaedic Trauma*, 8(3), 245–248.

Santos, R. R., Rahal, S. C., Neto, C. M., Ribeiro, C. R., Sousa, E. A. C., Foschini, C. R., Agostinho, F. S., and Mesquita, L. R. (2016). Biomechanical analysis of locking reconstruction plate using mono- or bicortical screws. *Materials Research*, 19(3), 588–593.

Sarwar, A., Gee, A., Bougherara, H., Kuzyk, P. R. T., Schemitsch, E. H., and Zdero, R. (2021). Biomechanical optimization of the far cortical locking technique for early healing of distal femur fractures. *Medical Engineering & Physics*, 89, 63–72.

Snow, M., Thompson, G., and Turner, P. G. (2008). A mechanical comparison of the locking compression plate (LCP) and the low contact-dynamic compression plate (DCP) in an osteoporotic bone model. *Journal of Orthopaedic Trauma*, 22(2), 121–125.

Wagner, M. (2003). General principles for the clinical use of the LCP. *Injury*, 34(Suppl. 2), B31–B42.

Wang, H., Liu, J., Wen, G., and Xie, Y. M. (2020). The robust fail-safe topological designs based on the von Mises stress. *Finite Elements in Analysis and Design*, 171, 103376.

Xiong, Y., Zhao, Y., Wang, Z., Du, Q., Chen, W., and Wang, A. (2009). Comparison of a new minimum contact locking plate and the limited contact dynamic compression plate in an osteoporotic fracture model. *International Orthopaedics*, 33(5), 1415–1419.

Xue, R., Lai, Q., Xing, H., Zhong, C., Zhao, Y., Zhu, K., Deng, Y., and Liu, C. (2024). Finite element analysis and clinical application of 3D-printed Ti alloy implant for the reconstruction of mandibular defects. *BMC Oral Health*, 24(1), 95.

Zhang, Y., Shao, Q., Yang, C., Ai, C., Zhou, D., Yu, Y., and Sun, G. (2021). Finite element analysis of different locking plate fixation methods for the treatment of ulnar head fracture. *Journal of Orthopaedic Surgery and Research*, 16(1), 191.